Journal of Sound and Vibration (1999) **226**(1), 169–187
Article No. jsvi.1999.2285, available online at http://www.idealibrary.com on IDEAL®

A TIP-TILT ADAPTIVE OPTICS SYSTEM FOR AMATEUR ASTRONOMERS AND OPTIMUM PLACEMENT OF ACTUATORS

PARTHAPRATIM CHAKRABORTY

Shiva Technologies Inc., 1510 *Drew Road*, *Unit* 10&11, *Mississauga*, *ON*, *Canada L5S* 1*W*7

KAMRAN BEHDINAN

Department of Mechanical Engineering, *Ryerson Polytechnic University*, *Toronto*, *ON*, *Canada M5B* 2*KS*

AND

BEHROUZ TABARROK

Department of Mechanical Engineering University of Victoria, *Canada*

(*Received* 4 *August* 1998, *and in final form* 1 *April* 1999)

A major concern in the design of a tip-tilt adaptive optics system, for amateur astronomical telescopes, is to find optimum positions of the actuators that result in least distortions of the mirror surface. A semi-analytical approach has been used, wherein the mirror is modelled as a thin circular plate with a peripheral ring mass and an elastic edge support. Modal analysis is performed to determine the natural frequencies and mode shapes of the system. The results of the modal analysis are incorporated in the subsequent harmonic analysis, where the response of the system to harmonic forces, applied by the three actuators, is expressed in terms of the Green functions. For various positions of the actuators, the maximum distortions on the mirror surface are evaluated, and from these results, the optimum positions of the actuators are located. The semi-analytical results are vertified by purely numerical results obtained from finite element analysis.

1. INTRODUCTION

Despite many adavancements achieved over the years in the design of telescopes, the ground-based telescopes still cannot match the resolution of space telescopes, due to the presence of turbulent atmosphere in the path of light. Thus, telescopes in space, for above the turbulent atmosphere were, until recently, regarded as the only means of obtaining clear images. However, now developments in Adaptive Optics (AO) have enabled astronomers to achieve image quality very close to that of the space telescopes [1, 2].

0022-460X/99/360149 + 19 $30.00/0

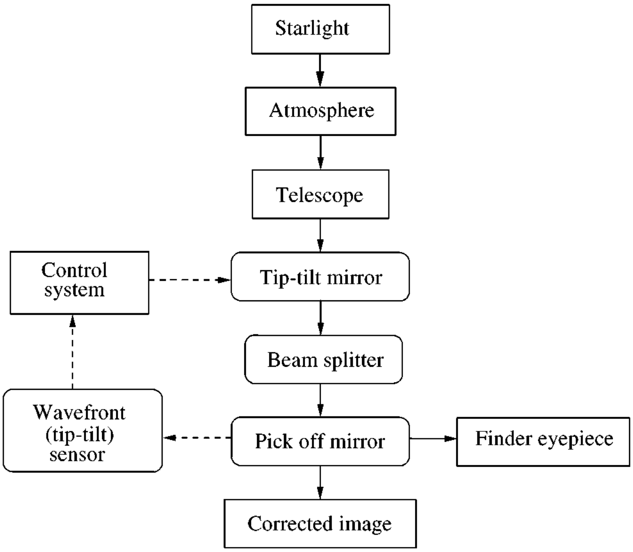

Figure 1. Schematic representation of the tip-tilt adaptive optics system.

As shown in Figure 1, the main elements of a tip-tilt adaptive optics system are the tip-tilt mirror, the wavefront sensor, the beam splitter and the control system. The AO system is mounted between the output of the telescope and the point where the image is observed. The position of the object measured by the wavefront sensor is fed into the control system which processes the information and controls the tip-tilt mirror to eliminate the motion of the object.

The tip-tilt mirror is designed to tip and tilt about two axes at a frequency as high as 100 Hz, without significant surface deformations. Thus, a major concern in the design of the tip-tilt system is to ensure that the optical surface of the mirror does not deform significantly (25×10^{-6} in maximum [3]) as a result of vibrations as otherwise the image quality would suffer. Therefore, it is important to find optimum positions for the actuators for minimum surface deformations

The finite element method (FEM) may be used to analyze the surface deformations of the mirror due to harmonic forces applied by the actuators, but this purely numerical approach becomes time-consuming and hence expensive when the placement of the actuators becomes part of the optimization process. Therefore, an alternative semi-analytical approach is used here, wherein the mirror is modelled as a thin circular plate, carrying a ring mass (the mass of the frame) and an elastic edge support, as well as three interior actuators. Modal analysis is carried out to derive the Green functions at the locations of the actuators. Then the response of the plate to harmonic forces applied by the actuators is expressed in terms of these Green functions.

Once the optimum position of the actuators is obtained, the actual deformation of the mirror surface may be found by a finite element analysis of the mirror.

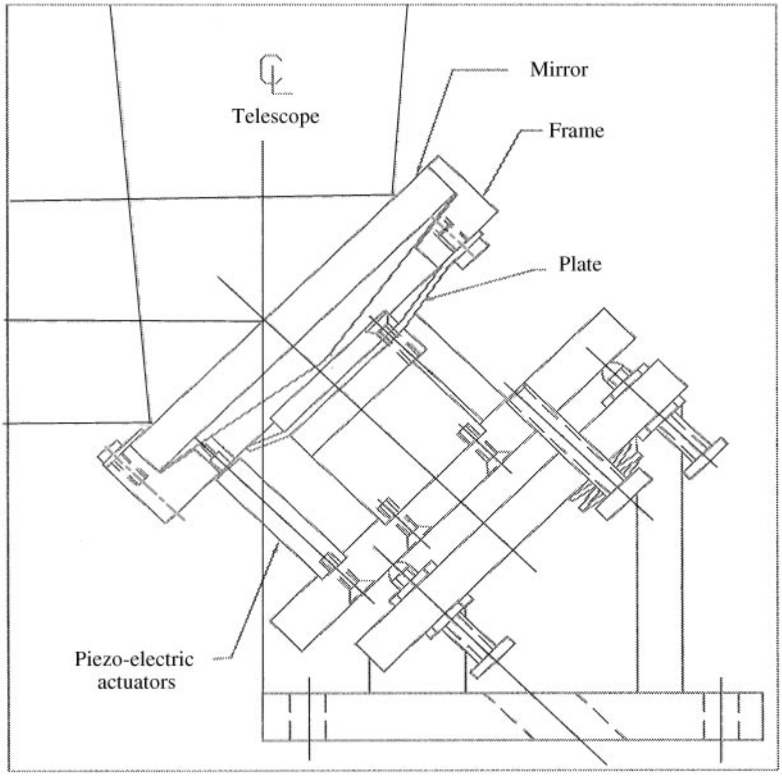

Figure 2. The tip-tilt mirror assembly.

2. SYSTEM OVERVIEW

The target telescopes for this AO system are in the range of 15–25 in diameter (with a focal ratio of $F/4{\cdot}5$) and are meant for use by amateur astronomers.

The tip-tilt mirror assembly is shown in Figure 2. The diameter of the mirror is 2·652 in and its thickness varies from 0·46 in at the center to 0·25 in at the periphery. The material selected for the mirror is Zerodur-543561 [4] because of its lower weight to stiffness ratio as compared with other materials (e.g. Pyrex). For the material of the frame, two different materials re considered, namely poly-vinyl-chloride (PVC) and aluminium. The properties of these two materials are provided in Table 1.

The mirror is held in the frame with the help of three evenly spaces brass clips. The frame is attached to a triangular stainless-steel plate, which is again fixed to the base plate. The triangular plate acts as a spring support for the mirror and the frame, and it holds the frame in place during the tip-tilt motion. For the analysis of the mirror assembly, it is necessary to incorporate the stiffness of this triangular plate spring. This was done using the ANSYS finite element program.

The finite element model of the plate spring is shown in Figure 3. The stiffness of the plate was evaluated as 12 246 lb/in. For further analysis of the mirror and the frame assembly, this triangular plate spring was replaced by an equivalent system of three linear springs with a stiffness of 4082 lb/in each.

TABLE 1

Material properties for the mirror and its frame

Properties	Symbol	Mirror	Frame
Material		Zerodur-543561*	Poly-vinyl chloride
Elastic limit (psi)	E	$13{\cdot}6 \times 10^6$	$6{\cdot}0 \times 10^5$
Density (lb/in^3)	ρ	0·0914	0·055
Poisson's ratio	ν	0·24	0·4

* Reference [4].

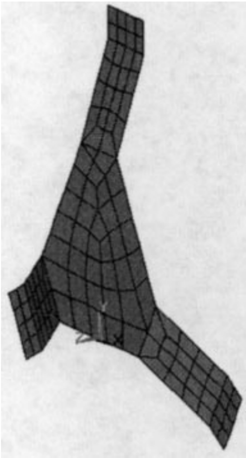

Figure 3. Finite element model of the plate spring.

3. ANALYTICAL FORMULATION

Vibration analysis of plates with various shapes and boundary conditions have been well documented by Leissa [5].

Axisymmetrical vibration of a circular plate with an elastic edge beam and a central mass was considered by Goel [6]. He obtained exact solutions in terms of Bessel functions for the natural frequencies, and showed the effects of varying the ratio of the concentrated mass to the mass of the plate and the stiffness of the edge beam to the stiffness of the plate, on the eigenfrequencies of the system.

Achong [7] used the Rayleight–Ritz technique to obtain an approximate solution for the natural frequencies of vibrating, elastically restrained, circular plates, with a ring mass along the edge and a concentrated mass at the centre. Numerical examples presented for various mass loading and support conditions are shown to be in agreement with values obtained by other methods.

The vibration of circular plates supported by combinations of ring and line supports and carrying concentrated masses was investigated by Liew [8] and Liew and Lim [9]. He used the Rayleight–Ritz method to approximate the mode shapes of continuous circular plates with various edge supports and interior annular and/or line supports.

Nicholson and Bergman [10, 11] considered the case of simply supported thick square plates carrying concentrated masses, and expressed the response of the system to harmonic motion in terms of the Green functions.

Azimi [12] used the modal expansion technique and the recptance method (essentially the same as the Green function method) for the free vibration analysis of circular plates with elastic or rigid interior supports on concentric circles in the plate.

LeClair [13] followed the same approach as Nicholson and Bergman or Azimi. He determined the natural frequencies and mode shapes for a circular plate with free edge and with three simple, interior supports. He determined the Green functions for the free vibration of a free edge circular plate by modal analysis, and used the same to derive the characteristic equation and mode shapes for a free-edge circular plate with three interior, simple supports

In the present study, we follow the methods of Nicholson and Bergman [10, 11] and Azimi [12]. The response of the system to harmonic forces applied by the three actuators is expressed in terms of the Green functions obtained by the modal analysis. The displacements are prescribed at the locations of the three actuators, and the displacement on the plate surface is expressed in terms of the Green functions. The surface deformation which is the difference between the calculated displacement amplitude and the rigid-body deflection, is calculated for various positions of the actuators (the three actuators being on a concentric circle), and the optimum position of the actuators for the minimum surface deformation is then determined.

3.1. MODAL ANALYSIS OF A CIRCULAR PLATE WITH A RING MASS AND ELASTIC EDGE SUPPORT

The differential equation for the free vibration of a thin circular plate of radius "a" and thickness $h(\ll b)$ is given by [14]

$$D\nabla^4\, w(r,\theta,t) + \rho h\,\frac{\partial^2 w}{\partial t^2}(r,\theta,t) = 0, \tag{1}$$

where ρ is the mass density and ∇^2 is the Laplacian operator.

The flexural rigidity of the plate is

$$D = Eh^3/12(1-v^2),$$

where E is the Young modulus and v is the Poisson ratio of the material of the mirror.

Using the method of separation of variables,we can express the general solution for the normal modes as [15]

$$W_{nj}(r,\theta) = R_{nj}(r)\,\Theta_{nj}(\theta) = \left[\mathrm{J}_n\left(\frac{\lambda_{nj} r}{a}\right) + \kappa_{nj}\,\mathrm{I}_n\left(\frac{\lambda_{nj} r}{a}\right)\right] \times (A_{nj}\cos(n\theta) + B_{nj}\sin(n\theta)), \tag{2}$$

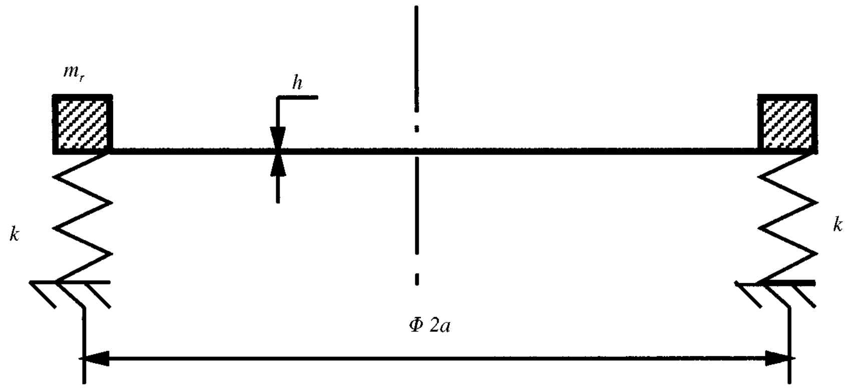

Figure 4. An elastically supported circular plate of radius a carrying a peripheral ring mass

where $n \geqslant 0$ for $j > 0$ and $n \geqslant 2$ for $j = 0$; J_n represents the Bessel function of the first kind of order n, and I_n denoted the modified Bessel function of the first kind of order n, and $\lambda_{nj}^2 = \omega_{nj} a^2 \sqrt{\rho h / D}$, where ω_{nj} is the natural frequency.

The right-body modes ($\omega_{nj} = 0$) corresponding to $n = 0$, 1 take the form [16]

$$W_{n0} = \left(\frac{r}{a}\right)^n [A_{n0} \cos(n\theta) + B_{n0} \sin(n\theta)] \tag{3}$$

the values of λ_{nj} can be obtained by applying the boundary conditions. For a plate with peripheral ring mass (m_r) and elastic edge support (stiffness of the support being k) (see Figure 4), the boundary conditions can be written as

$$(M_r)_{r=a} = 0: \quad -D\left[\frac{\partial^2 w}{\partial r^2} + \nu\left(\frac{1}{r}\frac{\partial w}{\partial r} + \frac{1}{r^2}\frac{\partial^2 w}{\partial \theta^2}\right)\right] = 0 \tag{4}$$

$$(V)_{r=a} = -\frac{m_r}{2\pi a}\frac{\partial^2 w}{\partial t^2}_{r=a} - kw,$$

i.e.

$$-\frac{\partial}{\partial r}[D(\nabla^2 w)] - \frac{1}{r}\frac{\partial}{\partial \theta}\left[(1-\nu)D\left(\frac{1}{r}\frac{\partial^2 w}{\partial r \partial \theta} - \frac{1}{r^2}\frac{\partial w}{\partial \theta}\right)\right] = -\frac{m_r}{2\pi a}\frac{\partial^2 w}{\partial t^2} - kw. \tag{5}$$

Substitution of equations (2) into equations (4) and (5) and application of the recurrence formulae for Bessel functions [17] result in the following characteristic equation for λ_{nj}:

$$\frac{[\lambda_{nj}^2 - n(n-1)(1-\nu)]\ \mathrm{J}_n(\lambda_{nj}) - (1-\nu)\ \lambda_{nj}\ \mathrm{J}_{n+1}(\lambda_{nj})}{[\lambda_{nj}^2 + n(n-1)(1-\nu)]\ \mathrm{I}_n(\lambda_{nj}) - (1-\nu)\ \lambda_{nj}\ \mathrm{I}_{n+1}(\lambda_{nj})}$$
$$= \frac{[n\lambda_{nj}^2 + n^2(n-1)(1-\nu) - \frac{\zeta}{2}\ \lambda_{nj}^4 + \Gamma]\,\mathrm{J}_n(\lambda_{nj}) - \lambda_{nj}[\lambda_{nj}^2 + n^2(1-\nu)]\,\mathrm{J}_{n+1}(\lambda_{nj})}{[n\lambda_{nj}^2 - n^2(n-1)(1-\nu) + \frac{\zeta}{2}\ \lambda_{nj}^4 - \Gamma]\,\mathrm{I}_n(\lambda_{nj}) + \lambda_{nj}[\lambda_{nj}^2 - n^2(1-\nu)]\,\mathrm{I}_{n+1}(\lambda_{nj})} \tag{6}$$

Here, $\zeta = m_r / \rho h \pi a^2$ is the mass ratio and $\Gamma = ka^3/D$ is referred to as the stiffness ratio [6, 7].

TABLE 2

Values of $\lambda_{nj}^2 = \omega_{nj} a^2 \sqrt{\rho h/D}$ for a circular plate ($\nu = 0{\cdot}3$) with peripheral ring mass (mass ratio $= \zeta$) and elastic edge-support

	ζ							
Γ	$\zeta = 0{\cdot}0$	$\zeta = 0{\cdot}01$	$\zeta = 0{\cdot}1$	$\zeta = 0{\cdot}25$	$\zeta = 1{\cdot}0$	$\zeta = 2{\cdot}5$	⋮	∞
1	1·37373 (1·374)*	1·36766	1·31617	1·24126	0·992578	0·816361	⋮	
10	3·45066 (3·451)*	3·44492	3·39314	3·30675	2·90151	2·5776	⋮	4·93515 (4·935)*
100	4·72865 (4·729)*	4·72843	4·72639	4·72293	4·70391	4·675540	⋮	
∞	←	—	4·93515 (4·935)*	—	—	→	⋮	

*Reference [12] values.

The values of λ_{nj}^2 (corresponding to the lowest natural frequency) for different values of ζ and Γ obtained by solving the above characteristic equation are listed in Table 2 and compared with published values wherever available. Figures 5–7 show the three modes of variation of λ_{nj}^2 with ζ and Γ for a circular plate with Poisson's ratio of 0·33, respectively. From Table 2 and Figures 5–7 it is evident that when both ζ and Γ vanish, the system corresponds to the case of a free-edge circular plate. On the other hand, for very large values of the ring mass or stiffness of the spring support (i.e., as $\zeta \to \infty$ or $\Gamma \to \infty$), the system becomes equivalent to the case of a circular plate simply supported around the periphery. Thus, the present system is neither completely free, nor simply supported, but somewhere in between these two extremes.

Values of λ_{nj}^2 ($n, j \leqslant 9$) for the mass ratio of $\zeta = 0{\cdot}38$ are provided in Table 3.

The amplitude parameter A_{nj} (or B_{nj}) can be evaluated by applying the orthogonality condition of the modes as

$$\int_0^{2\pi}\int_0^a \rho h W_{nj} W_{kl}\, r\,\mathrm{d}r\,\mathrm{d}\theta = (m + m_r)\,\delta_{nk}\delta_{jl}, \tag{7}$$

where $m = \pi\rho h a^2$ is the total mass of the plate, m_r the ring-mass and δ_{nk} the Kronecker delta.

Substituting from equations (2) and (3) into equation (7), we obtain the values of A_{nj} (for $\zeta = 0{\cdot}38$), presented in Table 4.

3.2. HARMONIC ANALYSIS OF THE PLATE WITH THREE ACTUATORS

The differential equation for forced vibration of circular plates is

$$D\nabla^4 w(r, \theta, t) + \rho h \frac{\partial^2 w}{\partial t^2}(r, \theta, t) = p(r, \theta, t), \tag{8}$$

where p is the transverse load per unit area of the plate.

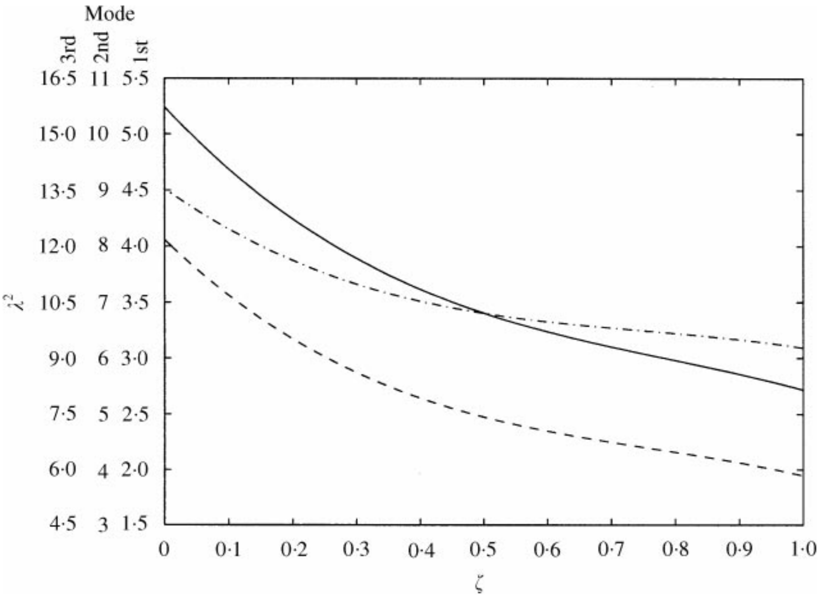

Figure 5. Frequency parameter, λ_{nj}^2, versus mass ratio, ζ (stiffness ratio $\Gamma = 0$); ———, 1st mode; ·–·–·–, 2nd mode; – – – 3rd mode.

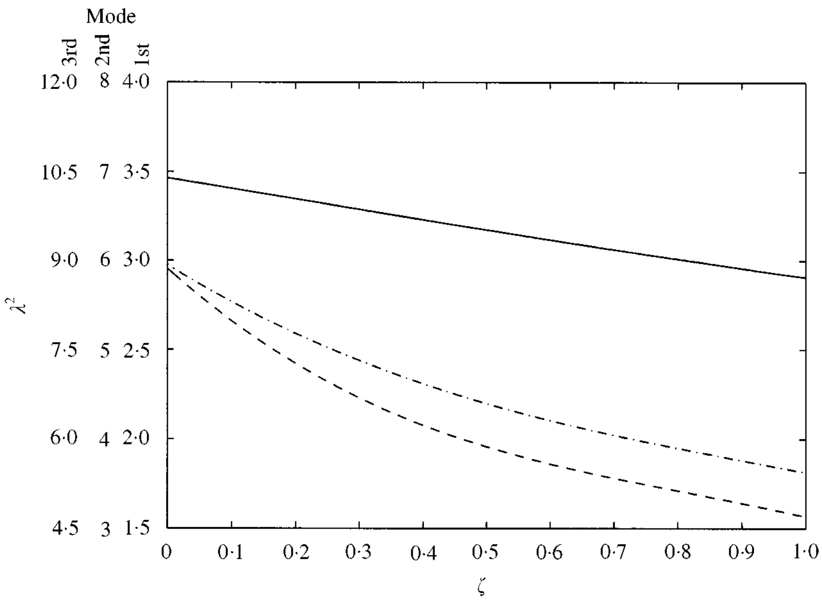

Figure 6. Frequency parameter, λ_{nj}^2, versus mass ratio, ζ (stiffness ratio $\Gamma = 10$); ——, 1st mode; ._._._, 2nd mode; – – – 3rd mode.

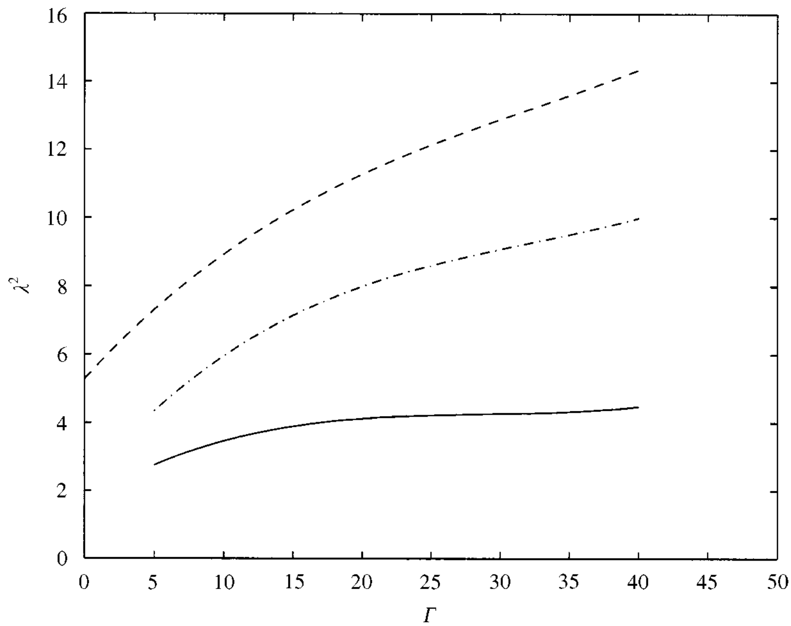

Figure 7. Frequency parameter, λ_{nj}^2, versus stiffness ratio, Γ ——, 1st mode; ._._._, 2nd mode; (mass ratio $\zeta = 0$); --- 3rd mode.

TABLE 3

Values of $\lambda_{nj}^2 = \omega_{nj} a^2 \sqrt{\rho h/D}$ *for a circular plate with ring mass nd elastic edge support*; $\nu = 0{\cdot}24$, $\zeta = 0{\cdot}38$, $\Gamma = 0{\cdot}1055$

j	$n = 0$	$n = 1$	$n = 2$	$n = 3$	$n = 4$
0	0·0000	0·489565	3·93306	8·56965	14·3461
1	6·946457	16·6979	29·290	44·4449	62·0553
2	32·7397	51·9253	74·0210	98·8984	126·473
3	77·7485	106·613	138·416	173·077	210·531
4	142·254	180·896	222·483	266·962	314·284
5	226·376	274·837	326·245	380·560	437·746
6	330·169	388·469	449·715	513·878	580·929
7	453·658	521·808	592·903	666·920	743·836
8	596·859	674·865	755·815	839·691	926·473
9	759·780	847·646	938·455	1032·19	1128·84

j	$n = 5$	$n = 6$	$n = 7$	$n = 8$	$n = 9$
0	21·1364	28·8411	37·3935	46·7230	56·7814
1	82·0620	104·4262	129·120	156·123	185·418
2	156·681	189·475	224·817	262·672	303·015
3	250·728	293·621	339·174	387·153	438·129
4	364·405	417·288	472·899	531·206	592·183
5	497·768	560·592	626·189	694·530	765·591
6	650·838	723·578	799·122	877·446	958·525
7	823·627	906·268	991·737	1080·01	1171·07
8	1016·14	1108·67	1204·05	1302·26	1403·26
9	1228·38	1330·80	1436·08	1544·20	1655·14

TABLE 4

Values of $A_{nj}^2 =$ for a circular plate with ring mass and elastic edge support; $v = 0{\cdot}24$, $\zeta = 0{\cdot}38$, $\Gamma = 0{\cdot}1055$

j	$n=0$	$n=1$	$n=2$	$n=3$	$n=4$
0	1·0000	7·88362	13·9065	20·3070	26·8442
1	5·52000	21·9057	34·2624	47·1672	60·3099
2	32·6531	28·6434	40·9000	53·8190	66·9896
3	67·9974	35·6778	47·6600	60·5422	73·7152
4	128·625	42·9317	54·5254	67·3282	80·4820
5	233·40·8	50·3791	61·4897	74.1760	87·2893
6	416·477	58·0068	68·5500	81·0839	94·1382
7	740·177	65·8067	75·7048	88·0523	101·0·293
8	1319·96	73·7711	82·9516	95·0806	107·961
9	2372·42	81·8947	90·2887	102·1685	114·937

j	$n=5$	$n=6$	$n=7$	$n=8$	$n=9$
0	33·4596	40·1247	46·8225	53·5436	60·2810
1	73·5867	86·9483	100·3666	113·825	127·312
2	80·2914	93·6724	107·105	120·576	134·072
3	87·0267	100·4177	113·860	127·338	140·840
4	93·7908	107·184	120·630	134·112	147·619
5	100·5838	113·971	127·417	140·898	154·405
6	107·406	120·780	134·219	147·697	161·203
7	114·258	127·612	141·039	154·510	168·013
8	121·141	134·468	147·877	161·340	174·834
9	128·056	141·347	154·735	168·181	181·667

The three actuators at $p(b, \alpha)$, $q(c, \beta)$ and $r(d, \gamma)$ (see Figure 8) produce harmonic forces of frequency Ω and unknown magnitudes P, Q and R, resulting in the forcing term

$$p(r, \theta, t) = [P\delta(r-b)\,\delta(\theta-\alpha) + Q\delta(r-c)\delta(\theta-\beta) + R\delta(r-d)\delta(\theta-\gamma)]\ \mathrm{d}^{\mathrm{i}\Omega t}, \quad (9)$$

where $\mathrm{i} = \sqrt{-1}$.

Using separation of variables and representing the deflection as a series of the vibration modes,

$$w(r, \theta, t) = \sum_{n=0}^{\infty} \sum_{j=0}^{\infty} W_{nj}(r, \theta) f_{nj}(t). \quad (10)$$

and substituting equations (9) and (10) in equation (8), we obtain

$$\sum_{n=0}^{\infty} \sum_{j=0}^{\infty} W_{nj}(r, \theta) \left[\frac{d^2 f_{nj}(t)}{\mathrm{d}t^2} + \omega_{nj}^2 f_{nj}(t) \right] = [P\delta(r-b)\delta(\theta-\alpha) + Q\delta(r-c)\delta(\theta-\beta) + R\delta(r-d)\delta(\theta-\gamma)]\,\mathrm{e}^{\mathrm{i}\Omega t}. \quad (11)$$

Equation (11) can now be solved by following the procedure described by Volterra and Zachmanoglou [15]. Using equations (2) and (3) and multiplying both sides of

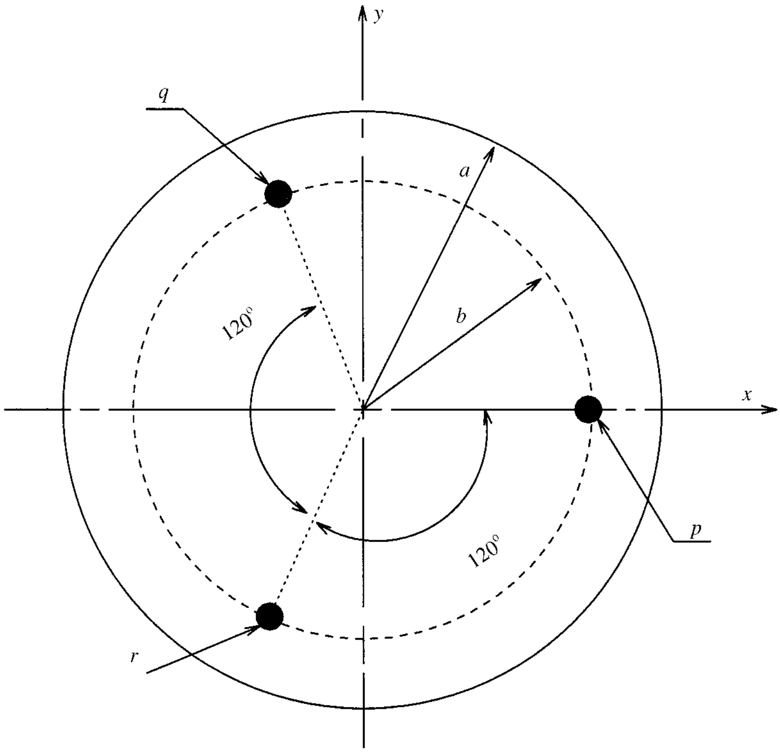

Figure 8. A circular plate of radius a with three actuators on a concentric circle of radius b.

equation (1) by $A_{mn} R_{mn}(r) \cos(m\theta)$, and integrating over the area of the plate, we obtain

$$\frac{d^2 f_{nj}(t)}{dt^2} + \omega_{nj}^2 f_{nj}(t) =$$

$$\frac{P A_{nj} R_{nj}(b) \cos(n\alpha) + Q A_{nj} R_{nj}(c) \cos(n\beta) + R A_{nj} R_{nj}(d) \cos(n\gamma)}{\pi a^2 h \rho} \mathrm{e}^{i\Omega t}. \quad (12)$$

Similarly, multiplying equation (11) by $B_{mn} R_{mn}(r) \sin(m\theta)$, integrating over the area of the plate and using the orthogonality relations for normal modes, we find

$$\frac{d^2 f_{nj}(t)}{dt^2} + \omega_{nj}^2 f_{nj}(t) =$$

$$\frac{P B_{nj} R_{nj}(b) \sin n\alpha + Q A_{nj} R_{nj}(c) \sin n\beta + R A_{nj} R_{nj}(d) \sin n\gamma}{\pi a^2 h \rho} \mathrm{e}^{i\Omega t}. \quad (13)$$

Combining equations (12) and (13) and noting that $A_{nj} = B_{nj}$ for $n \geqslant 1$ and $j \geqslant 0$ and $B_{0j} = 0$, we may solve equations (12) and (13) for f_{nj} which when substituted in equation (11) gives

$$w(r, \theta, t) = [P G_p(r, \theta) + Q G_q(r, \theta) + R G_r(r, \theta)] \mathrm{e}^{i\Omega t}, \quad (14)$$

where G_p, G_q and G_r are the Green functions [10, 11] corresponding to the forces P, Q and R, respectively and are given by

$$G_p(r,\,\theta) = \sum_{n=0}^{\infty}\sum_{j=0}^{\infty} \frac{A_{nj}^2 R_{nj}(b) R_{nj}(r) \cos[n(\theta-\alpha)]}{\pi a^2 h\rho(\omega_{nj}^2 - \Omega^2)},$$

$$G_q(r,\,\theta) = \sum_{n=0}^{\infty}\sum_{j=0}^{\infty} \frac{A_{nj}^2 R_{nj}(c) R_{nj}(r) \cos[n(\theta-\beta)]}{\pi a^2 h\rho(\omega_{nj}^2 - \Omega^2)},$$

$$G_p(r,\,\theta) = \sum_{n=0}^{\infty}\sum_{j=0}^{\infty} \frac{A_{nj}^2 R_{nj}(d) R_{nj}(r) \cos[n(\theta-\gamma)]}{\pi a^2 h\rho(\omega_{nj}^2 - \Omega^2)}. \tag{15}$$

3.2.1. *Tilt about x-axis*

For tilting motion about the x-axis, the displacement at location p (see Figure 8) is zero. If the tilt is prescribed, equation (14) will yield the following set of equations:

$$PG_{pp} + QC_{pq} + RG_{pr} = 0,\ PG_{qp} + QG_{qq} + RG_{qr} = A,\ PG_{rp} + QG_{rq} + RG_{rr} = -A. \tag{16}$$

where A is the magnitude of the prescribed initial displacement at q and r, while G_{pq} denotes the Green function of a force at a point p and evaluated at q.

Since the actuators are symmetrically placed, using partial sums as approximations for the infinite series involved in the expression for the Green functions, we write

$$G_1 = G_{pp} = G_{qq} = G_{rr} = \sum_{n=0}^{N-1}\sum_{j=0}^{J-1} \frac{A_{nj}^2 R_{nj}^2(b)}{\pi a^2 h\rho(\omega_{nj}^2 - \Omega^2)},$$

$$G_2 = G_{pp} = G_{qr} = G_{rp} = \sum_{n=0}^{N-1}\sum_{j=0}^{J-1} \frac{A_{nj}^2 R_{nj}^2(b) \cos[2\pi n/3]}{\pi a^2 h\rho(\omega_{nj}^2 - \Omega^2)}. \tag{17}$$

Then equations (16) can be solved for P, Q and R as

$$P = 0, \qquad Q = -R = \frac{A}{G_1 - G_2}. \tag{18}$$

Therefore, the lateral displacement on the mirror surface can be written from equation (14) as

$$w(r,\,\theta,\,t) = [QG(r,\,\theta,\,\beta;\,\Omega) + RG(r,\,\theta,\,\gamma;\,\Omega)]\,\mathrm{e}^{\mathrm{i}\Omega t}, \tag{19}$$

where Q and R are given by equation (18) and

$$G(r,\,\theta,\,\beta;\,\Omega) = \sum_{n=0}^{N-1}\sum_{j=0}^{J-1} \frac{A_{nj}^2 R_{nj}(b) R_{nj}(r) \cos[n(\theta-\beta)]}{\pi a^2 h\rho(\omega_{nj}^2 - \Omega^2)},$$

$$G(r,\,\theta,\,\gamma;\,\Omega) = \sum_{n=0}^{N-1}\sum_{j=0}^{J-1} \frac{A_{nj}^2 R_{nj}(b) R_{nj}(r) \cos[n(\theta-\gamma)]}{\pi a^2 h\rho(\omega_{nj}^2 - \Omega^2)},$$

3.2.2. *Tilt about y-axis*

If the prescribed displacement at p is assumed as B, the corresponding displacement prescribed at each of the location q and r will be $-B/2$. Then we may derive from equation (14), in the manner described above and find

$$P = \frac{B}{(G_1 - G_2)}, \qquad Q = R = -\frac{B}{2(G_1 - G_2)} \tag{20}$$

The corresponding response of the mirror will be

$$w(r, \theta, t) = [PG(r, \theta, \alpha; \Omega) + QG(r, \theta, \beta; \Omega) + RG(r, \theta, \gamma; \Omega)]\, e^{i\Omega t}. \tag{21}$$

4. RESULTS AND DISCUSSION

The deformations of the top surface of the plate can be evaluated by substracting the values of rigid-body deflection from the total surface deflections. Evidently, the maximum surface deformation depends upon the positions of the actuators.

Figures 9 and 10 show the surface deformation patterns for tilt about the x- and y-axies respectively.

As noted earlier the material of the mirror is assumed to be Zerodur-543561 [4] with $E = 13{\cdot}6 \times 10^6$ psi, $\rho = 0{\cdot}0914$ lb/in^3 and $\nu = 0{\cdot}24$. The infinite series in the expressions for Green functions were approximated using ten terms, i.e., $N = J = 10$.

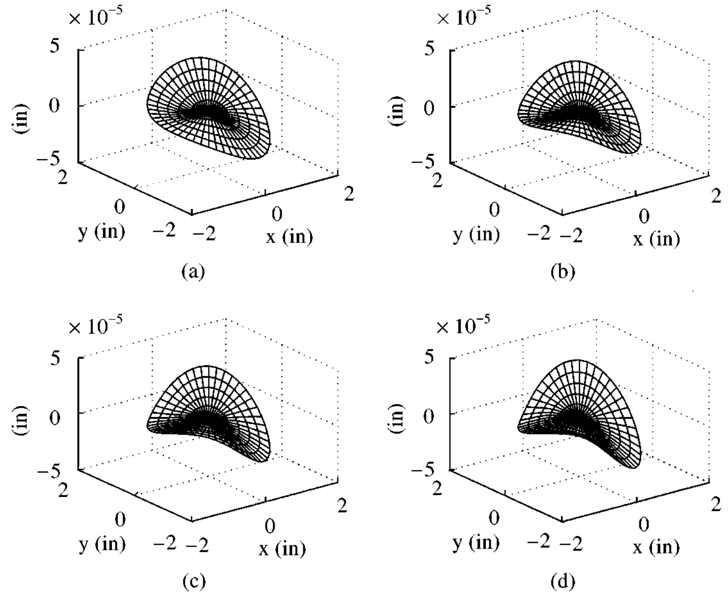

Figure 9. Actual deformation of the plate surface for various positions of the actuators: (a) $b/a = 1/3$, (b) $b/a = 1/2$, (c) $b/a = 2/3$ and (d) $b/a = 5/6$; $D = 2{\cdot}652$ in, $h = 0{\cdot}3$ in, tilt angle $= 3{\cdot}5 \times 10^{-4}$ rad and frequency of vibration $= 100$ Hz about the x-axis.

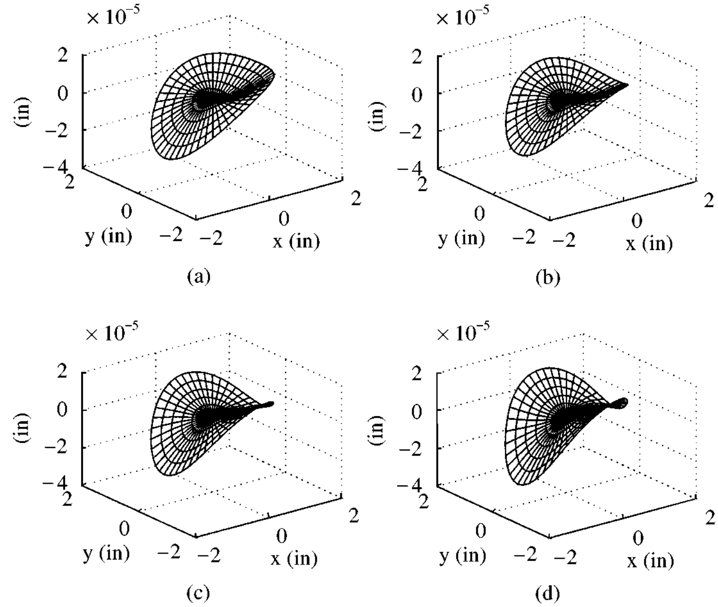

Figure 10. Actual deformation of the plate surface for various positions of the actuators: (a) $b/a = 1/3$, (b) $b/a = 1/2$, (c) $b/a = 2/3$ and (d) $b/a = 5/6$; $D = 2{\cdot}652$ in, $h = 0{\cdot}3$ in, tilt angle $= 2{\cdot}5 \times 10^{-4}$ rad and frequency of vibration = 100 Hz about the y-axis.

For the solution of the characteristic equation (6), the IMSL Version 1.1 subroutine ZERAL and for evaluating the Bessel functions, IMSL version 1.0 subroutines BSJNS and BSINS were used.

For various positions of the actuators (i.e., for various b/a ratios), maximum values of surface deformations were calculated and the results are presented in Figures 11–16. We have presented the results only for two forcing frequencies, namely 70 Hz and 100 Hz. For 50 Hz frequency, it was not feasible to determine any optimum positions since the forcing frequency is too far removed from the fundamental frequency of the plate to excite the system.

For the purpose of verifying the results obtained here, a harmonic analysis of the mirror was carried out using the ANSYS finite element programme. In the finite element analysis, the mirror was modelled as a flat circular plate consisting of 72, 20–node brick elements with wedge-shaped elements near the centre. A circular frame is attached to the mirror along its periphery. Although, in the physical model, the three springs attached to the frame are symmetrically placed, here, we have placed the springs around the periphery of the frame/mirror to render the FE model similar to the analytical model.

It can be seen that the "equivalent FEM" (with distributed elastic support all around the periphery) which is equivalent to our analytical model, show essentially the same results as the "actual FEM". The analytical results deviate from the FE results for positions of actuators close to the centre of the mirror. This is due to the fact that the thin plate model in the analytical calculations ignores the effects of shear deformations and thus underestimates the deformation. However, the

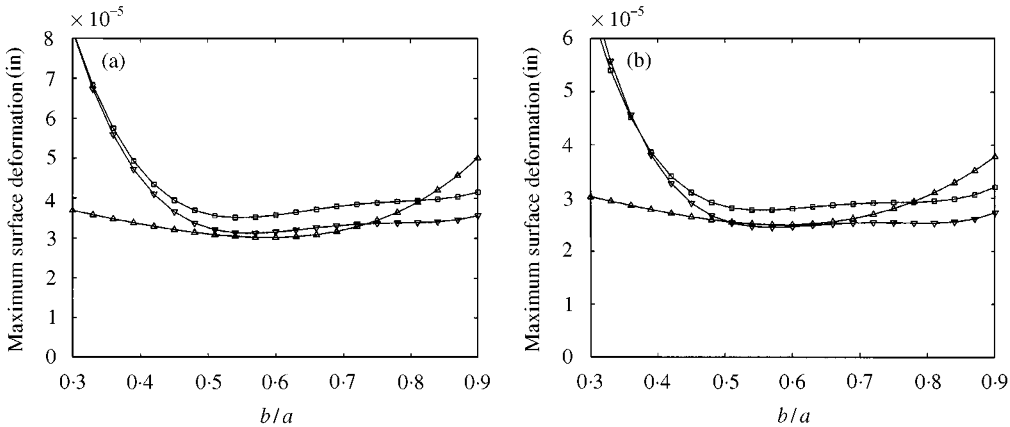

Figure 11. Variation of maximum surface deformation of the plate with positions of the actuators: $D = 2{\cdot}652$ in, $h = 0{\cdot}3$ in, $\zeta = 0{\cdot}25$, forcing frequency = 100 Hz; (a) for tilt angle of $3{\cdot}5 \times 10^{-4}$ about the x-axis; (b) for tilt angle of $2{\cdot}5 \times 10^{-4}$ about the y-axis; $\triangle$, analytical; $\square$, equivalent FEM; ∇, actual FEM.

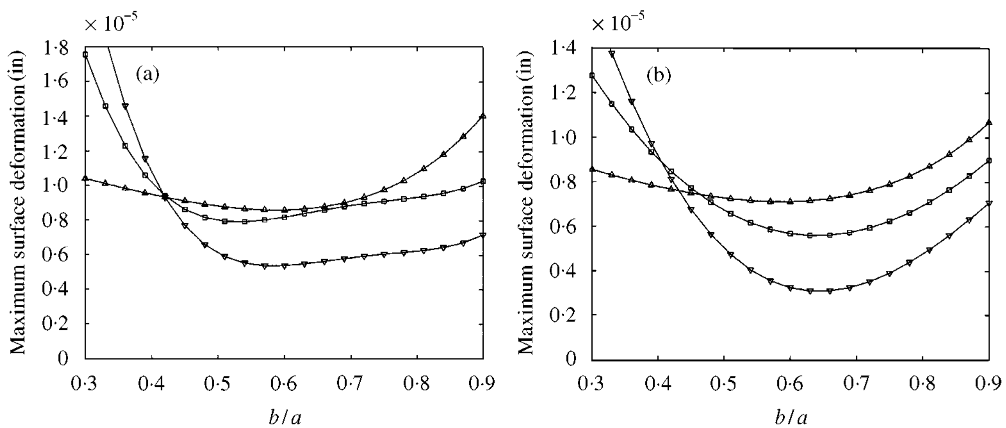

Figure 12. Variation of maximum surface deformation of the plate with positions of the actuators: $D = 2{\cdot}652$ in, $h = 0{\cdot}3$ in, $\zeta = 0{\cdot}25$, forcing frequency = 70 Hz; (a) for tilt angle of $3{\cdot}5 \times 10^{-4}$ about the x-axis; (b) for tilt angle of $2{\cdot}5 \times 10^{-4}$ about the y-axis; $\triangle$, analytical; $\square$, equivalent FEM; ∇, actual FEM.

analytical model predicts the same optimum position for the actuators as the FEM and also the difference between the analytical and FEA results is least at the optimum position.

Hence, the semi-analytical method is useful for locating the optimum radial position of the actuators for which the surface deformation would be relatively low. Once the optimum position is located, the actual value of the surface deformation my be easily calculated using a single model on ANYS.

It is also interesting to note, from Figures 11–16, that the optimum position of the actuators shift further away from the centre as the mass ratio, ζ (i.e., ratio of the mass of the frame to the mass of the mirror) is increased. For example, from

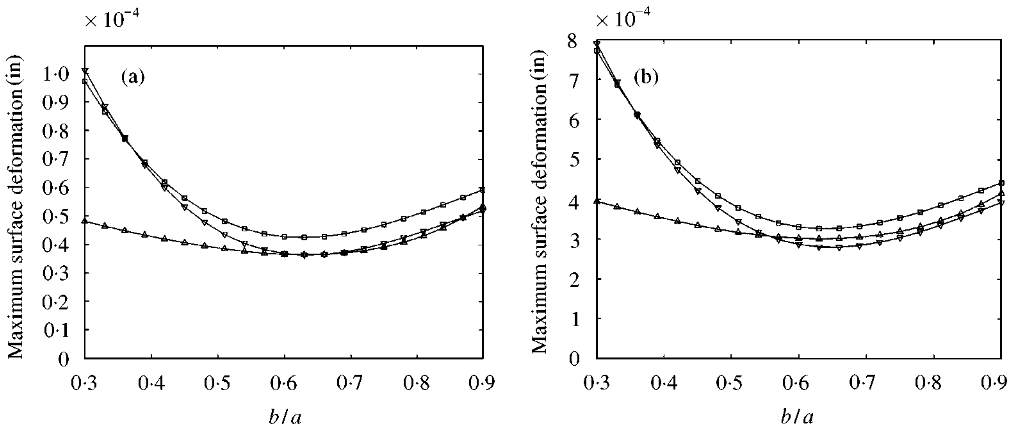

Figure 13. Variation of maximum surface deformation of the plate with positions of the actuators: $D = 2{\cdot}652$ in, $h = 0{\cdot}3$ in, $\zeta = 0{\cdot}38$, forcing frequency = 100 Hz; (a) for tilt angle of $3{\cdot}5 \times 10^{-4}$ about the x-axis; (b) for tilt angle of $2{\cdot}5 \times 10^{-4}$ about the y-axis; $\triangle$, analytical; $\square$, equivalent FEM; ∇, actual FEM.

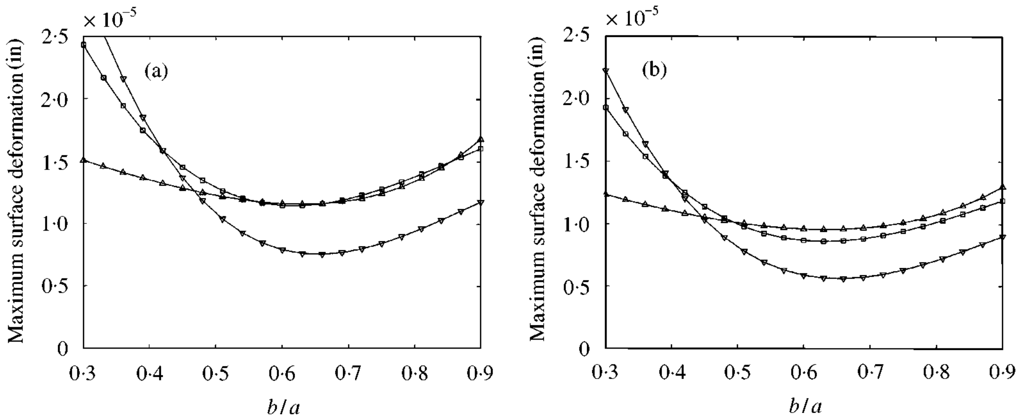

Figure 14. Variation of maximum surface deformation of the plate with positions of the actuators: $D = 2{\cdot}652$ in, $h = 0{\cdot}3$ in, $\zeta = 0{\cdot}38$, forcing frequency = 70 Hz; (a) for tilt angle of $3{\cdot}5 \times 10^{-4}$ about the x-axis; (b) for tilt angle of $2{\cdot}5 \times 10^{-4}$ about the y-axis; $\triangle$, analytical; $\square$, equivalent FEM; ∇, actual FEM.

Figures 11, 13 and 15, for three different mass ratios (but all at the same frequency of 100 Hz and for tilt about the x-axis), it can be seen that as the mass ratio is increased from $\zeta = 0{\cdot}25$ to 0·66, the optimum position of the actuators increases from approximately $b/a = 0{\cdot}55$ at $\zeta = 0{\cdot}25$ to $b/a = 0{\cdot}66$ at $\zeta = 0{\cdot}38$ and $b/a = 0{\cdot}8$ at $\zeta = 0{\cdot}66$. For sufficiently high mass ratio ($\zeta > 1$), the actuators should be placed at the periphery of the mirror to keep the deformations low. From the design point of view, it is desirable to place the actuators as close as possible to the centre, where the displacements are the smallest and the cost of the stacked piezxoelectric actuators would thus be least. Hence, we have selected PVC for the frame material (for which $\zeta = 0{\cdot}38$) instead of aluminium (for which $\zeta = 0{\cdot}66$).

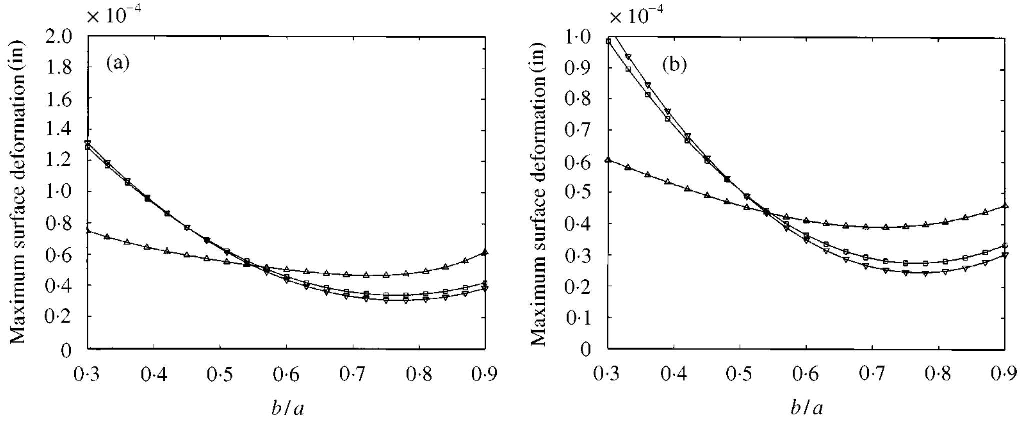

Figure 15. Variation of maximum surface deformation of the plate with positions of the actuators: $D = 2{\cdot}652$ in, $h = 0{\cdot}3$ in, $\zeta = 0{\cdot}66$, forcing frequency = 100 Hz; (a) for tilt angle of $3{\cdot}5 \times 10^{-4}$ about the x-axis; (b) for tilt angle of $2{\cdot}5 \times 10^{-4}$ about the y-axis; $\triangle$, analytical; $\square$, equivalent FEM; ∇, actual FEM.

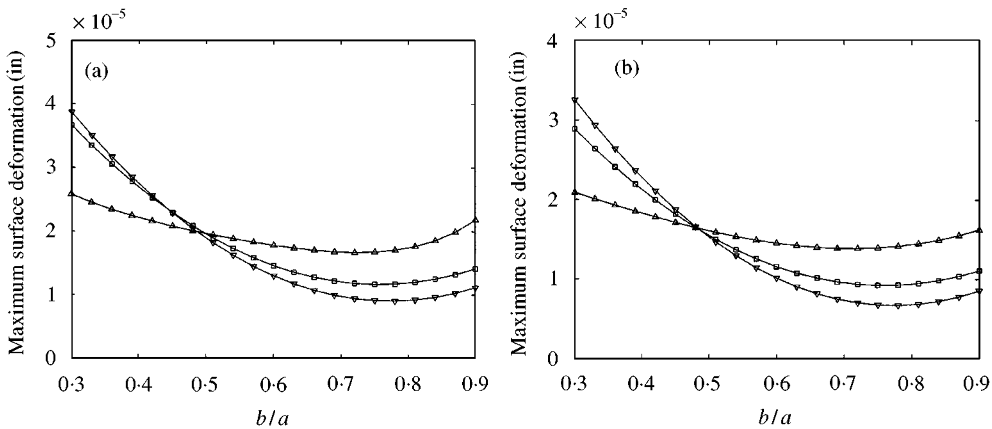

Figure 16. Variation of maximum surface deformation of the plate with positions of the actuators: $D = 2{\cdot}652$ in, $h = 0{\cdot}3$ in, $\zeta = 0{\cdot}66$, forcing frequency = 70 Hz; (a) for tilt angle of $3{\cdot}5 \times 10^{-4}$ about the x-axis; (b) for tilt angle of $2{\cdot}5 \times 10^{-4}$ about the y-axis; $\triangle$, analytical; $\square$, equivalent FEM; ∇, actual FEM.

It can be seen from, Figures 13 and 14 that the optimum position of the actuators for our model of the mirror and frame assembly (i.e., for mirror material being Zerodur and frame material being PVC) is at two-third the radius of the mirror.

Also, the deformation on the top surface of the mirror, corresponding to this optimum position is equal to $41{\cdot}75 \times 10^{-6}$ in (for tilt about the x-axis), which is higher than the allowable value of 25×10^{-6} in. However, the plate surface deformations for 50 and 70 Hz frequencies are found to be $4{\cdot}5 \times 10^{-6}$ and $9{\cdot}12 \times 10^{-6}$ in, respectively, well below the acceptable limit.

5. CONCLUDING REMARKS

The present study was carried out in aid of design for a tip-tilt adaptive optics (AO) system for small-scale telescopes used by amateur astronomers and small professional observatories. A major concern in the deign of tip-tilt mirrors is that the distortion of the top surface of the mirror should be kept as low as possible (optical design requirement is approx. 25×10^{-6} in maximum) to improve the image quality. A semi-analytical approach has been developed and discussed here for the harmonic analysis of the mirror assembly. The mirror is modelled as a circular plate with a peripheral rings mass (equal to the mass of the frame) and elastic edge support, and with three interior actuators. The mode shapes obtained from the model analysis have been incorporated in the forced vibration analysis to evaluate the response of the system to harmonic forces applied by the three actuators. The response of the system has been expressed in terms of Green functions. The displacements were prescribed at the locations of the actuators, and the lateral displacements on the mirror top surface were calculated for various positions of the actuators.

The results obtained by the semi-analytical method have been shown to be in good agreement with the FE results, especially near the optimum positions.

The investigation was carried out for three different mass ratios ζ (mass of frame to the mass of mirror). It has been observed that as ζ increases, the actuators must be moved farther away from the centre for optimum positions. For example, the optimum position of the actuators for $\zeta = 0{\cdot}38$ (corresponding to a PVC frame) is about two-third the diameter of the mirror, while for $\zeta = 0{\cdot}66$ (corresponding to an aluminium frame) it is about 80% of the diameter of the mirror. Since the cost of the piezoelectic stack depends on the amount of displacement required, PVC (with $\zeta = 0{\cdot}38$) has been selected as the material of the frame to keep the cost of actuators low, for a mirror of diameter 2·652 in made of Zerodur-5453561.

ACKNOWLEDGMENT

Funding for this project, provided by the Natural Science and Engineering Research Council of Canada, is gratefully acknowledged.

REFERENCES

1. J. M. Beckers 1993 *Annual Rev. Astronomy and Astrophysics* **31**, 13–62. Adaptive optics for astronomy: principles, performance and applications.
2. L. E. Schmutz 1993 *Photonics Spectra* 119–122. Adaptive optics: a modern cure for Newton's tremors.
3. A. Ahmad (editor) 1997 *Handbook of Optomechanical Engineering*. New York: CRC Press, Inc.
4. P. R. Yoder, Jr. 1986 *Opto-Mechanical Systems Design*. New York: Marcel Dekker.
5. A. W. Leissa 1993 *Vibration of Plates*. Columbus, OH: Acoustical Society of America, American Institute of Physics.
6. R. P. Goel 1975 *Journal of Sound and Vibration*, **41**, 85–91. Axisymmetrical vibration of a circular plate having an elastic edge-beam and a central mass.

7. A. Achong 1995 *Journal of Sound and Vibration* **183**, 157–168. Vibrational analysis of circular and elliptical plates carrying point and ring masses and with edges elastically restrained.
8. K. M. Liew 1992 *Journal of Sound and Vibration* **156**, 99–107. Vibration of eccentirc ring and line supported circular plates carrying concentrated masses.
9. K. M. Liew and C. W. Lim 1994 *Journal of Sound and Vibration* **170**, 412–414. Authors' reply.
10. J. W. Nicholson and L. A. Bergman 1985 *Journal of Sound and Vibration* **103**, 357–369. Vibration of thick plates carrying concentrated masses.
11. J. W. Nicholson and L. A. Bergman 1985 *Journal of Sound and Vibration* **98**, 299–30. On the efficacy of the modal series representation for the Green functions of vibrating continuous structures.
12. S. Azimi 1988 *Journal of Sound and Vibration* **120**, 37–52. Free vibration of circular plaes with elastic or rigid interior support.
13. R. A. Leclair 1993 *Journal of Sound and Vibration* **160**, 289–300. Modal analysis of circular plates with a free edge and three simple interior supports.
14. W. Soedel 1981 *Vibration of Shells and Plates*. New York: Marcel Dekker.
15. E. Volterra and E. C. Zachmanoglou 1965 *Dynamics of Vibration*. Columbus, OH: Charles E. Merrill.
16. K. Itao and S. H. Crandall 1979 *Journal of Aplied Mechanics* **46**, 448–453. Natural modes and natural frequencies of uniform, circular, free-edge plates.
17. N. W. McLachlan 1948 *Bessel Functions for Engineers*, Oxford Engineering Science Series. Oxford: Oxford University Press.